Pergamon

*Int. J. Heat Mass Transfer.* Vol. 38, No. 4, pp. 615–627, 1995

0017-9310/95 $9.50+0.00

0017-9310(94)00201-0

# An analytical model for local heat transfer coefficients for forced convective condensation inside smooth horizontal tubes

M. S. CHITTI and N. K. ANAND†

Department of Mechanical Engineering, Texas A&M University, College Station, TX 77843, U.S.A.

(*Received* 29 *October* 1993 *and in final form* 1 *July* 1994)

**Abstract**—An analytical model based on annular flow is proposed for predicting the local heat transfer coefficient for forced convective condensation inside smooth horizontal tubes. The Prandtl mixing length theory, Van-Dreist's hypothesis and Reynolds analogy are used for the analysis. Experiments are conducted by condensing R-22 inside an 8.001 mm (0.315 in.) i.d. copper tube for a wide range of mass flux rates and condensing temperatures. The analytical results, compared with the experimental data and four other correlations reported in the literature indicate that 80% of the predictions are within ±25% of the experimental data, with a mean deviation of 15.3%.

## INTRODUCTION

Forced convective condensation inside horizontal tubes is widely adopted in process industries, refrigeration, and air-conditioning equipment. The analysis of heat transfer in such applications is extremely important for designing the condensers. Mostly, the designer is interested in predicting the two-phase heat transfer coefficient (film coefficient) for a given set of flow conditions. Since the film coefficient is known to vary along the length of the condenser due to changes in the flow patterns, it is desirable to predict the local values. However, pure theoretical treatment of the two-phase flow during condensation is very difficult. Hence most of the times, empirical or semi-empirical models (using some of the experimental data) were developed which led to several existing correlations.

It is observed by many investigators that for high vapor velocities, annular flow is the predominant flow pattern during condensation inside tubes, even for qualities as low as 25% [1–3]. This simplifies the analysis of the condensation problem to a great extent. For the same reason, similar to the studies made earlier based on annular flow configuration, the present work is an attempt in the same direction.

Condensation heat transfer was extensively studied both for internal and external flow situations by several investigators. Most of the authors [4–15] have used a part of their experimental data in developing their analytical models which were based on annular flow. Also the literature survey reveals that very few studies [3, 16, 17] were made which have a pure theoretical basis.

Nusselt's [17] analysis of film condensation was the earliest and a fundamental one for different situations such as vertical and inclined plates and outside horizontal tubes (external flow) and vertical tubes (internal flow). But several of his assumptions such as constant wall temperature, linear temperature distribution in the liquid film and condensate laminar flow, in many applications, were shown to give erroneous results by Jakob [18]. Later Carpenter and Colbourn [19] assuming turbulent flow in the liquid film, showed that the main resistance to heat transfer was offered by the laminar sublayer and estimated its thickness too. Akers *et al.* [5, 6] studied the effects of vapor velocity and the fluid properties on the average heat transfer coefficient of a condensing vapor inside a horizontal tube, using an equivalent liquid mass velocity ($G_e$). Boyko and Kruzhilin [10] used a similar analysis for steam condensation inside tubes and developed a heat transfer correlation based on the analogy between the heat transfer and hydraulic resistance.

Analytical studies of a few authors such as Abis [4], Azer *et al.* [20], Bae *et al.* [8, 9], Kunz and Yerazunis [16], and Traviss *et al.* [21], match closely to that of the present work. All of them similar to the present authors except Kunz and Yerazunis [16], used the Von-Karman's equations of turbulent flow in pipes to represent the (universal) velocity distribution in the liquid film. In addition, the turbulent Prandtl number ($Pr_t$) was used to link the governing momentum and energy equations thus requiring to solve only one combined equation. This is due to the fact that $Pr_t$ is the ratio of eddy diffusivities for heat transfer ($\varepsilon_h$) and momentum ($\varepsilon_m$).

The objective of the present study is to suggest an alternative calculation procedure for determining the local heat transfer coefficient for annular flow condensation inside horizontal tubes. The current model differs from others in evaluating the quantity $\varepsilon_m$ for

†Author to whom correspondence should be addressed.

## NOMENCLATURE

| | |
|---|---|
| $A$ | surface area [$m^2$ ($ft^2$)] |
| $C_p$ | refrigerant specific heat at constant pressure [J $kg^{-1}$ $K^{-1}$(Btu $lbm^{-1}$ $°F^{-1}$] |
| $e$ | error in the heat transfer coefficient |
| $F_{TD}$ | flow regime transition parameter [defined in equation (27)] |
| $G$ | liquid refrigerant mass flux rate [kg $m^{-2}$ $s^{-1}$ (lbm $hr^{-1}$ $ft^{-2}$)] |
| $G_e$ | equivalent mass velocity, $G_v(\rho_l/\rho_v)^{1/2}+G_l$ [kg $m^{-2}$ $s^{-1}$ (lbm $hr^{-1}$ $ft^{-2}$)] |
| $h$ | convective heat transfer coefficient [W $m^{-2}$ $K^{-1}$ (Btu $hr^{-1}$ $ft^{-2}$ $°F^{-1}$)] |
| $j$ | superficial mass velocity [m $s^{-1}$ (ft $hr^{-1}$)] |
| $k$ | thermal conductivity of the refrigerant [W $m^{-1}$ $K^{-1}$ (Btu $hr^{-1}$ $ft^{-1}$ $°F^{-1}$)] |
| $K$ | thermal conductivity of copper refrigerant tube [W $m^{-1}$ $K^{-1}$ (Btu $hr^{-1}$ $ft^{-1}$ $°F^{-1}$)] |
| $L$ | length [m (ft)] |
| $Pr$ | Prandtl number |
| $\lvert dP/dz \rvert$ | pressure gradient [Pa $m^{-1}$ (psi $ft^{-1}$)] |
| $q$ | heat flux [W $m^{-2}$ (Btu $hr^{-1}$ $ft^{-2}$)] |
| $r$ | radius [m (ft)] |
| $T$ | temperature [°C or K (°F)] |
| $U$ | overall heat transfer coefficient [W $m^{-2}$ $K^{-1}$ (Btu $hr^{-1}$ $ft^{-2}$ $°F^{-1}$) |
| $u$ | friction velocity [m $s^{-1}$ (ft $hr^{-1}$)] |
| $W$ | mass flow rate of the refrigerant [kg $s^{-1}$ (lbm $hr^{-1}$)] |
| $x$ | quality at any location $z$ |
| $y$ | distance from the tube wall [m (ft)] |
| $z$ | axial location [m (ft)]. |

Subscripts

| | |
|---|---|
| av | mean |
| calc | calculated |
| e | equivalent |
| exp | experimental |
| h | heat transfer |
| i | inside of refrigerant tube |
| l | liquid refrigerant |
| m | momentum |
| o | evaluated at the tube wall surface |
| o | outside of refrigerant tube [equation (C4)] |
| T | total for mass flow rate $W$ |
| TPF | two-phase friction |
| v | refrigerant vapor |
| $x$ | at a quality $x$. |

Superscripts

| | |
|---|---|
| * | symbol for friction velocity, $u^* = \sqrt{(\tau_0/\rho_l)}$ |
| + | non-dimensional symbol. |

Greek symbols

| | |
|---|---|
| $\delta$ | film thickness [m (ft)] |
| $\mu$ | dynamic viscosity of the refrigerant [kg $m^{-1}$ $s^{-1}$ (lbm $hr^{-1}$ $ft^{-1}$)] |
| $v$ | kinematic viscosity of the refrigerant [$m^2$ $s^{-1}$ ($ft^2$ $hr^{-1}$)] |
| $\rho$ | density of the refrigerant [kg $m^{-3}$ (lbm $ft^{-3}$)] |
| $\tau$ | shear stress [N $m^{-2}$ (lbf $ft^{-2}$)] |
| $\phi_{vv}$ | Lockhart–Martinelli parameter defined in equation (16). |

which the Prandtl mixing length theory in combination with the Van-Driest's hypothesis [22] (for the law of the wall) is used. Also, other models involve evaluation of shear stress distribution, pressure drop and void fractions while the present model eliminates all these calculations. Also the model developed in this paper, unlike others, does not need any local experimental measurement data such as tube wall temperatures.

## ANALYTICAL MODEL

The physical model of the problem is shown in Fig. 1 and the following simplifying assumptions are made in the analysis.

(1) Annular flow configuration is assumed for the analysis. The flow pattern in most part of the condensation region in the condenser is observed to be annular flow for smooth horizontal tubes by several authors in their flow pattern studies [1–3].

(2) Annular flow implies that a thin liquid film is present and is attached to the tube wall around the circumference while the vapor core occupies the central portion of the tube. In other words film condensation is assumed.

(3) The thickness of the liquid film is assumed to be uniform all around the circumference of the tube.

(4) The assumption of uniform film thickness in

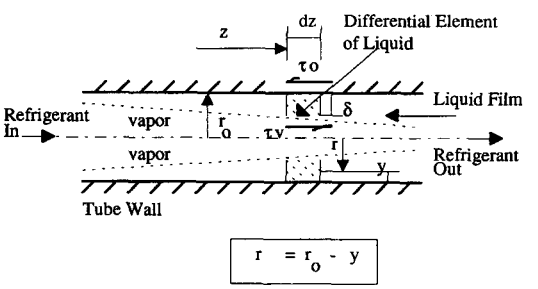


Fig. 1. Physical situation for the annular flow condensation.

the azimuthal direction simplified the problem to be axisymmetric and a one-dimensional one.

(5) Liquid entrainment in the vapor core region is neglected.

(6) Steady, turbulent flow in the liquid film is assumed.

(7) The liquid properties are assumed to be constant in the liquid film.

(8) Liquid subcooling in the liquid film is neglected.

(9) The turbulent Prandtl number ($Pr_t$) which is the ratio of eddy diffusivities for heat ($\varepsilon_h$) and momentum transfer ($\varepsilon_m$) is given a constant value of 0.9 [22].

(10) The vapor is at the saturation temperature.

The governing equations for momentum and heat transfer across the liquid film (see Fig. 1) during turbulent flow can be expressed as follows:

$$\tau = (\mu_l + \rho_l \varepsilon_m)\frac{du}{dy} \tag{1}$$

and

$$q = -(k_l + \rho_l C_{pl} \varepsilon_h)\frac{dT}{dy}. \tag{2}$$

The above equations (1) and (2) are the basic definitions of the total apparent shear stress (molecular + turbulent) and the total heat flux during turbulent flow. They can be expressed in an alternative form as follows:

$$\frac{\tau}{\rho_l} = (\nu_l + \varepsilon_m)\frac{du}{dy} \tag{3}$$

and

$$\frac{q}{\rho_l C_{pl}} = -(\alpha_l + \varepsilon_h)\frac{dT}{dy}. \tag{4}$$

Equations (3) and (4) can be written in a non-dimensionalized form as follows:

$$\frac{\tau}{\tau_0} = \left(1 + \frac{\varepsilon_m}{\nu_l}\right)\frac{du^+}{dy^+} \tag{5}$$

and

$$\frac{q}{q_0} = \left(\frac{1}{Pr} + \frac{\varepsilon_h}{\nu_l}\right)\frac{dT^+}{dy^+} \tag{6}$$

where the different non-dimensional terms are given as follows:

$$u^+ = \frac{u}{u^*} = \frac{u}{\sqrt{\tau_0/\rho_l}}$$

$u^* = \sqrt{\tau_0/\rho_l}$ is the friction velocity (7a)

$$y^+ = \frac{yu^*}{\nu_l} = \frac{y\sqrt{\tau_0/\rho_l}}{\nu_l} \tag{7b}$$

$$T^+ = \frac{(T_0 - T)u^*}{(q_0/(\rho_l C_{pl}))} \tag{7c}$$

and

$$Pr = \frac{\nu_l}{\alpha_l} = \frac{\mu_l C_{pl}}{k_l}. \tag{7d}$$

The two equations (5) and (6) can be combined into one by using the turbulent Prandtl number ($Pr_t$) which relates the turbulent eddy diffusivities for momentum ($\varepsilon_m$) and heat ($\varepsilon_h$) as given in equation (8) to obtain $T^+$ in terms of $y^+$, from which $h_x$ can be evaluated. For this purpose the Prandtl's mixing length ($l$) theory with Van-Dreist's hypothesis for '$l$' is used which gives $\varepsilon_m/\nu_l$ directly in terms of $y^+$. In addition, the Von-Karman's universal distribution of velocity, i.e. $u^+$ in terms of $y^+$ and $Pr_t = 0.9$ [22] are used. We have

$$Pr_t = \frac{\varepsilon_m}{\varepsilon_h} = \frac{\varepsilon_m/\nu_l}{\varepsilon_h/\nu_l}. \tag{8}$$

Using the above equation (8), the term $\varepsilon_h/\nu_l$ written in terms of $\varepsilon_m/\nu_l$ and $Pr_t$ is substituted into equation (6) to obtain

$$\frac{q}{q_0} = \left(\frac{1}{Pr} + \frac{1}{Pr_t}\left[\frac{\varepsilon_m}{\nu_l}\right]\right)\frac{dT^+}{dy^+}. \tag{9}$$

Separating the differentials of the variables $T^+$ and $y^+$ in equation (9) above and integrating in the radial direction from 0 to $y^+$, we get

$$T^+ = \int_0^{y^+}\left(\frac{(q/q_0)}{\left(\frac{1}{Pr} + \frac{1}{Pr_t}\left[\frac{\varepsilon_m}{\nu_l}\right]\right)}\right)dy^+. \tag{10}$$

Hence the temperature drop across the liquid film can be obtained from $T^+$ in above equation (10) by performing the integration from 0 to $\delta^+$. Calling that integral as $T_\delta^+$, we get

$$T_\delta^+ = \int_0^{\delta^+}\left(\frac{(q/q_0)}{\left(\frac{1}{Pr} + \frac{1}{Pr_t}\left[\frac{\varepsilon_m}{\nu_l}\right]\right)}\right)dy^+. \tag{11}$$

Using definition of $T_\delta^+$ in equation (7c), we get

$$T_\delta^+ = \frac{(T_0 - T_\delta)u^*}{(q_0/(\rho_l C_{pl}))}. \tag{12}$$

Using the above equation (12) and the definition of $h_x$, we get

$$h_x = \frac{q_0}{(T_0 - T_\delta)} = \frac{\rho_l C_{pl} u^*}{T_\delta^+}. \tag{13}$$

Equation (11) can be integrated provided we know the relations for $\varepsilon_m/\nu_l$ and $q/q_0$ in terms of $y^+$, and the film thickness $\delta$. It is here that the current model differs from that of Azer *et al.* [20], specifically in the evaluation of $\varepsilon_m$. As mentioned earlier, the current model uses the Van-Dreists's hypothesis (see Appendix A) whereas the other authors [20] used equation (3) and expressed it in terms of the shear stress ($\tau/\tau_0$). The shear stress ($\tau/\tau_0$) was evaluated using a force balance on a differential element of liquid. It involves the shear stress at the interface ($\tau_v$), the total pressure

drop, the average liquid and vapor velocities and the void fraction ($\alpha$). All these are not needed by the current model, and $q/q_0$ is obtained from heat flux continuity in the radial direction neglecting axial diffusion (see Appendix B) and $\delta$ from an iteration process.

Kunz and Yerazunis [16] also used Prandtl mixing length approach but their model differs from the current one in certain respects. They used the Nikuradze's variation of the mixing length in which the shear stress distribution ($\tau/\tau_0$) is also included. They had developed the model to suit a variety of conditions including single phase flow. But its verification was done only for vertical flow with others' experimental data and analytical models. Although they have suggested that their analysis is valid for horizontal flow as well, Azer *et al.* [20] mentioned that it is not since the shearing action on the liquid film was neglected. The argument was based on the fact that annular flow pattern cannot be maintained in horizontal flow unless the vapor velocity and its shearing action are high enough to maintain the liquid film. However, the present model does not need any such assumption. Further, the iteration procedure adopted also differs from that of the present model. With an assumed value of $\delta^+$, $\tau/\tau_0$ was evaluated in terms of the axial static pressure gradient and the gravitational force on the liquid and the inertia terms were neglected. This $\tau/\tau_0$, $\varepsilon_m/\nu_l$ mentioned earlier and equation (1) were used to solve for the velocity profile in the liquid film. The velocity distribution was in turn used to evaluate the flow rate which is known. The current approach uses Von-Karman's velocity distribution (equations (A5)–(A7) in Appendix A) which eliminates the need to solve for it.

Carey [23] also used the Prandtl mixing length theory and with some simplifying assumptions obtained a closed form solution for predicting local $h$ for condensation in vertical tubes. But he assumed a constant shear layer in the liquid film (implying $\tau/\tau_0 = 1$) which is good for a first order approximation, whereas no such assumption is made in the current model. Also, he assumed a weakly turbulent liquid film (i.e. a viscous film), whereas both the vapor and liquid are assumed to be in turbulent flow in the current study. This assumption resulting in $\varepsilon_m/\nu_l \ll 1$ allowed him to directly integrate equation (11) and obtain a closed from solution, whereas the current study relaxes this assumption and the integration is performed using a numerical scheme.

Tichy *et al.* [24] developed an analytical model using the Reynolds analogy by an energy balance at the liquid–vapor interface for condensation of oil–refrigerant mixtures. Although their model can be applied for pure refrigerants, it requires the knowledge of wall shear, void fraction and condenser tube wall temperature (obtained from the local measurements). The current analysis avoids the need of void fraction and local measurement data and hence is simpler to use.

After evaluating $T_\delta^+$ from equation (11), $h_x$ can be calculated from equation (13) provided we know the friction velocity $u^*$. In this study, $u^*$ is evaluated using the Lockhart–Martinelli parameter at any axial location $z$ where the quality is specified.

*Numerical scheme for '$\delta$'*

As mentioned earlier, the friction velocity needs to be evaluated to calculate the local heat transfer coefficient $h_x$. The computer program written in FORTRAN first evaluates $u^*$, uses the iteration scheme to calculate $T_\delta^+$ and then calculates $h_x$. Hence, this section describes the calculation procedure in the same order.

*Friction velocity* u*. We have the relation for $u^*$ from equation (7a) as

$$u^* = \sqrt{(\tau_0/\rho_l)}$$

We also have from the force balance on a small elemental length dz of the condenser, referring to Fig. 1,

$$\tau_0(2\pi r_0) = \left(\frac{dp}{dz}\right)_{TPF}(\pi r_0^2) \tag{14}$$

which can be simplified as

$$\frac{2\tau_0}{r_0} = \left(\frac{dp}{dz}\right)_{TPF}. \tag{15}$$

But, using the Lockhart–Martinelli parameter $\phi_{vv}$, $(dp/dz)_{TPF}$ can be expressed as

$$\left(\frac{dp}{dz}\right)_{TPF} = \phi_{vv}^2\left(\frac{dp}{dz}\right)_v. \tag{16}$$

Substituting the equation (16) into equation (15) and using the relation of $u^*$ given in equation (7a), the following relation can be obtained:

$$\frac{\tau_0}{\rho_l} = (u^*)^2 = \frac{r_0}{2\rho_l}\phi_{vv}^2\left(\frac{dp}{dz}\right)_v \tag{17}$$

where, from Azer *et al.* [20],

$$\phi_{vv} = 1 + 2.85X_{tt}^{0.523} \tag{18}$$

where $X_{tt}$ is given by

$$X_{tt} = \left(\frac{\mu_l}{\mu_v}\right)^{0.1}\left(\frac{1-x}{x}\right)^{0.9}\left(\frac{\rho_v}{\rho_l}\right)^{0.5} \tag{19}$$

and

$$\left|\frac{dp}{dz}\right|_v = \frac{0.143\mu_v^{0.2}W_v^{0.8}}{\rho_v D^{4.8}} \tag{20}$$

where

$$W_v = W_T \cdot x. \tag{21}$$

*Convergence.* Referring to Fig. 1 and from the continuity equation for the liquid layer, we obtain an expression for the liquid flow rate $W_l$ as

$$W_l = 2\pi\rho_l \int_0^{\delta} u(r_0 - y)\,dy. \quad (22)$$

Since, for a given quality $x$, we have

$$W_l = W_T \cdot (1-x) \quad (23)$$

equation (23) can be rewritten using $W_l$ from equation (22) to obtain

$$W_{T,calc} = \frac{2\pi\rho_l}{(1-x)} \int_0^{\delta} u(r_0 - y)\,dy. \quad (24)$$

Equation (24) can be written in the non-dimensionalized form as

$$W_{T,calc} = \frac{2\pi\rho_l v_l^2}{(1-x)u^*} \int_0^{\delta^+} u^+(r_0^+ - y^+)\,dy^+. \quad (25)$$

Equation (25) represents the total mass flow rate calculated at any axial location $z$ and the integral is evaluated and $W_{T,calc}$ compared with the given experimental value ($W_{T,exp}$) as a check for convergence, i.e.

$$\left|\frac{W_{T,exp} - W_{T,calc}}{W_{T,exp}}\right| \times 100 \leqslant 1.0. \quad (26)$$

As can be seen from the above equations, once the quality $x$ is specified at a given location $z$, along with the other parameters such as mass flow rate $W_{T,exp}$, saturation properties at the condensing temperature, the friction velocity $u^*$ can be calculated. Once the friction velocity $u^*$ is calculated, the next step is to calculate the film thickness $\delta$ for which the algorithm written in FORTRAN is explained below.

*The algorithm.*

(1) *An initial value for* $\delta^+$ is assumed. Usually a value greater than 30 is assumed since the Von-Karman's distribution has three different profiles (equations (A5)–(A7) in Appendix A), the third profile being valid for $y^+ > 30$.

(2) The quantities such as $r_0^+$ (to evaluate $q/q_0$ in the integral of equation (11)) are evaluated using the definition of $y^+$.

(3) The integral in the equation (11) is split into a sum of three integrals with limits for $y^+$ as given in equations (A5)–(A7) in Appendix A.

(4) The three integrals mentioned in step 3 are evaluated in sequence using the trapezoid rule. For a particular case, step sizes of 1.0, 5.0 and 4.0, respectively, are chosen for the three integrals and evaluated. They were later reduced until the percentage error in the integral value ($T_\delta^+$) is less than 1.0%. From this process, step sizes of 0.5, 2.5 and 1.0, respectively, are chosen for the three integrals as the preset values for all the other cases.

(5) With the calculated value of $T_\delta^+$, the local value of heat transfer coefficient, i.e. $h_x$ is calculated using the equation (13). Also, the percentage error in the analytical value of $h_x$ with respect to the experimental value is calculated.

(6) Convergence is checked using equation (26).

(7) If the percentage error is less than 1.0, then the convergence is declared. Then the values of $\delta$, $\delta^+$, $T_\delta^+$, $h_x$ along with their percentage errors are reported and the program execution is terminated. If the convergence is not met, then the program skips the step 7 and goes directly to step 8.

(8) If the percentage error is greater than 1.0, then a new value of $\delta^+$ is assumed. If the calculated mass flow rate ($W_{T,calc}$) is greater (lesser) than the experimental value ($W_{T,exp}$), then $\delta^+$ is decreased (increased) by a certain preset value, and the steps from 2 to 7 are repeated until convergence.

Hence the current method can be seen to have developed on a semi theoretical basis. The only empiricism involved is the constants in equation (18) for evaluating $\phi_{vv}$, which were obtained from empirical correlations. It is simpler to use when compared to the other models reported in the literature. For instance, no experimental values of local measurements are needed. Only the global parameters such as the mass flow rate, the geometrical parameters such as the tube diameter, and the refrigerant properties at the condensing temperature are required to determine the local heat transfer coefficients for a given quality. Further, no assumption of the slip characteristics is needed and the calculations of void fraction, vapor and liquid velocities, and shear stress distribution are eliminated.

## EXPERIMENTS

A two-phase loop is built for conducting the condensation experiments. Refrigerant 22 is used for calibrating the test setup. A wide range of mass flux rates and condensing temperatures are used for the tests. Table 1 shows the range of testing conditions.

*Test setup*

The test setup consists of four main loops, namely the refrigerant, chilled water, hot water and test condenser cooling water loops. The refrigerant at state 1 [see Figs. 2(a) and (b)] is pumped by the diaphragm-type liquid refrigerant pump (eliminates oil contamination; driven by a variable speed DC motor) to a higher pressure and temperature (state 2). The three by-pass lines [only one is shown in the Fig. 2(a)] at the discharge side of the pump enable to regulate the desired refrigerant flow rate in the system. A tangential turbine flow meter placed in line reads the volumetric flow rate in the form of DC voltage output. The refrigerant then passes through the preheater heat exchanger to come out as a saturated/superheated vapor (state 3). The heating tape which is wound around the tubing (serves as a superheater) heats the refrigerant to a desired superheated condition (state 3). It is then condensed in the test condenser to a saturated/subcooled condition (state 4). Sight glasses are provided at both ends of the condenser to visually inspect the refrigerant condition. The refrigerant then

Table 1. Range of experimental conditions for R-22

| Parameter | Range | Units |
|---|---|---|
| Refrigerant mass flow rate | 0.45–1.36 | kg $min^{-1}$ |
| | (60–180) | (lbm $hr^{-1}$) |
| Refrigerant mass flux | 148–450 | kg $m^{-2}$ $s^{-1}$ |
| | (109 000–332 000) | (lbm $hr^{-1}$ $ft^{-2}$) |
| Refrigerant inlet superheat | 0.28–11.11 | °C |
| | (0.5–20) | (°F) |
| Refrigerant outlet subcooling | 0.17–8.33 | °C |
| | (0.3–15) | (°F) |
| Refrigerant inlet quality | 1.0 | — |
| Refrigerant outlet quality | 0.0 | — |
| Refrigerant condensing pressure | 1241–1827 | kPa |
| | (180–265) | (psia) |
| Refrigerant condensing temperature | 32.2–51.7 | °C |
| | (90–125) | (°F) |
| Cooling water flow rate | 94.6–220.8 | $cm^3$ $s^{-1}$ |
| | (1.5–3.5) | (gpm) |

flows through a series of throttle valves to drop in the pressure from state 4 to state 5 and accumulates in the liquid receiver. It finally passes through the subcooler heat exchanger to reach the inlet of the refrigerant pump (state 1) and thus completes the cycle.

The chilled water is a water–glycol mixture (50% each by volume) maintained by a R-502 chiller unit. It is used to cool the refrigerant to a subcooled condition in the subcooling heat exchanger. The hot water is obtained through a 12 kW boiler and circulates through the 5 ton preheater to heat the refrigerant to a saturated/superheated vapor. The test condenser cooling water is obtained by a 1.5 kW water heater and its flow rate is controlled and measured by a 0–220.8 $cm^3$ $s^{-1}$ (0–3.5 gpm) rotameter. It picks up heat while condensing the refrigerant and is cooled by the water–glycol mixture of the chilled water loop.

*Test condenser*

The test condenser is basically a tube-in-tube heat exchanger with a counterflow arrangement, Fig. 3(a); the refrigerant flowing through the inner tube and the cooling water flowing through the annulus in the opposite direction. The inner tube is a 9.525 mm (3/8 inch) O.D. copper tube with a wall thickness of 0.762 mm (0.03 inches), while the outer tube is a 41.35 mm (1.625 inches) O.D. copper tube of 1.59 mm (1/16 inch) wall thickness. The test section is designed to allow local measurement at five locations along the length.

At each of the five locations along the test section, the refrigerant pressure, the refrigerant temperature, the temperature of the outside surface of the inner tube and the water temperature were measured [see Fig. 3(b)]. All the temperatures were measured by the T-type copper–constantan thermocouples and the pressures by SETRA pressure transducers. At each of the five locations, the surface temperature of the inner tube was measured at four points on the surface with thermocouples, 90 degrees apart and their arithmetic mean was taken to be the average surface temperature. The water temperature was measured by one thermocouple on each side of the inner tube placed at the center of the annulus region, facing the direction of water flow.

*Test procedure*

All the different instruments were calibrated before the tests are begun. The thermocouples were calibrated using a constant temperature bath and the pressure transducers with a dead weight tester. The flow meters (refrigerant, mass flow, turbine meters and the rotameter) were calibrated using water. The average error of the thermocouple was about 0.28°C (0.5°F), that of the pressure transducer was about 0.69 kPa (0.1 psi) and that of the flow meters was about 5–7%.

The system was charged with the correct amount of the refrigerant after checking for leaks. First the refrigerant and then the condenser water were circulated through the test section until stable flow was obtained. Then the hot water was circulated through the evaporation heat exchanger to heat the refrigerant to a saturated/superheated condition. The electric heating tape superheater was used (when necessary) to precisely control the inlet condition of superheated state of the refrigerant.

An ACUREX datalogger synchronized to a personal computer was used to record the data through 57 channels. The test setup was run for a considerable amount of time until stable values were observed. When all the values did not vary by more than 1% of their readings for about 10 min, a steady state was said to have reached. The energy balance was said to have achieved when the difference in the energy gained by the cooling water and the energy lost by the refrigerant during condensation was less than 10%. Tests for which the energy balance was more than 10% were rejected although they had reached the stable flow conditions. The data was collected for about 10 min at every 15 s time interval.

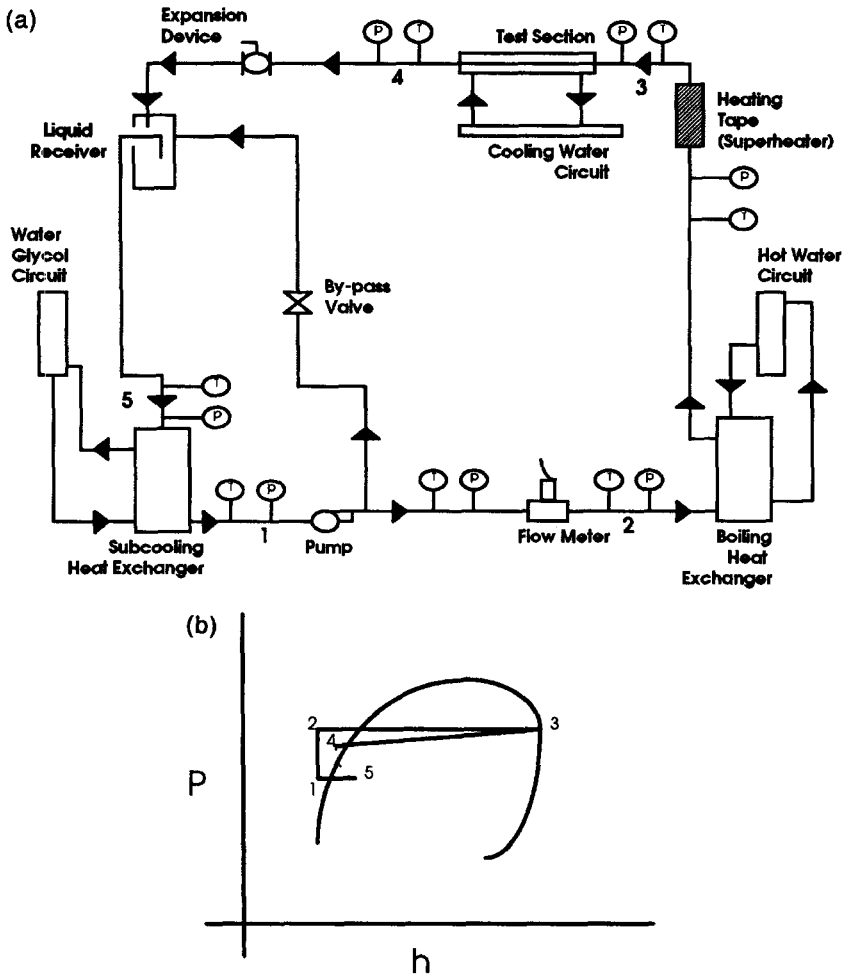


Fig. 2. Schematic of the test apparatus and thermodynamic path of the refrigerant: (a) schematic of the test apparatus; (b) thermodynamic path of the refrigerant.

A FORTRAN program was written for post-processing the data to average the readings, calculate the experimental pressure drop, the local and average heat transfer coefficients. The local heat transfer coefficient was calculated at three innermost locations. At each of these three points, the measurements at the neighboring locations were used, the distance considered as the length of the heat exchanger.

The one-dimensional conduction model, the (sensible) heat gain by the flowing water and the logarithmic mean temperature difference were used in calculating the heat transfer coefficient. The calculations were made using six chosen correlations also. All the refrigerant properties were calculated using the Martin–Hou equation of state (Downing [25]; Kartsounes and Erth [26]).

For the uncertainty analysis, the recent guidelines proposed by Kim *et al.* [27] were followed although the basic methodology of Kline and McClintock [28] was adopted (see Appendix C and Chitti [29] for a detailed discussion). From the analysis, it was found that the average uncertainty in the measurement of the heat transfer coefficient was $\pm 25\%$.

## RESULTS AND DISCUSSION

Figure 4 shows the flow regime transitions for four tests plotted using the flow pattern map suggested by Taitel and Dukler [3]. The four tests are in the increasing order of mass flux rate and represent the total range of the experimental conditions used in this study. All the curves are drawn for the parameter $F_{TD}$ as a function of Lockhart–Martinelli parameter ($\phi_{vv}$) which depends on local quality and saturation properties of the condensing fluid. The parameter $F_{TD}$ indicates the transition from stratified wavy to dispersed annular flow or stratified wavy to intermittent (plug/slug flow). It is a measure of the superficial vapor flux relative to that of the gravitational force acting on the liquid that causes the liquid to flow at the bottom of the tube and is evaluated by

$$F_{TD} = \left[\frac{\rho_v j_v^2}{(\rho_l - \rho_v) Dg \cos \Omega}\right]^{1/2}. \quad (27)$$

In the above equation, the numerator and denominator represent the superficial vapor flux and the gravitational force on the liquid, respectively. Also in

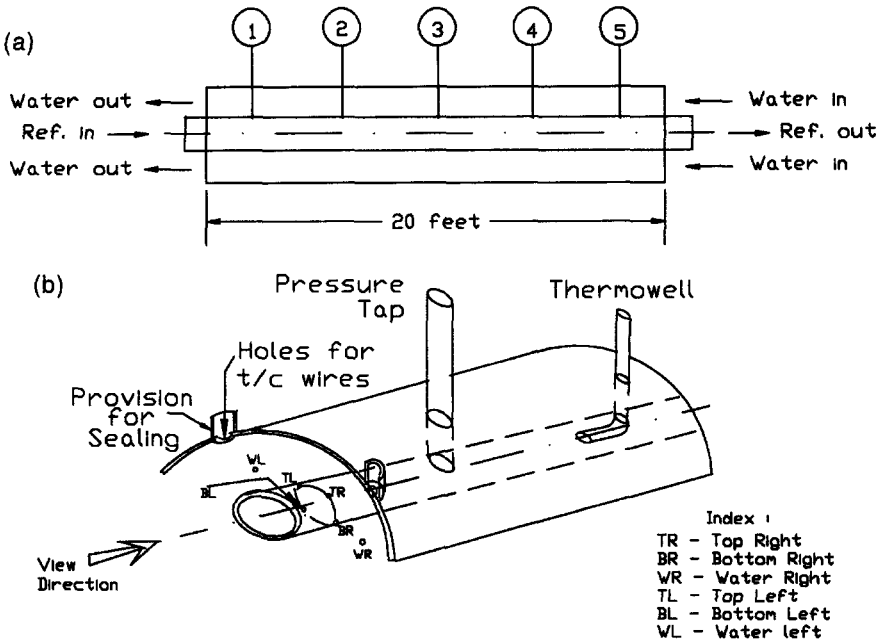


Fig. 3. Details of local measurement technique: (a) locations of local measurement along the test section; (b) variables of local measurement.

the current study, $\Omega$, the angle of inclination of the condenser tube with the horizontal is zero ($\cos\Omega = 1$) since the tube is horizontal. For the four tests plotted,

| | Run | G kg/ sq.m s (lbm/hr sq.ft) | P(sat) kPa (psia) | T(sat) deg. C (deg. F) | Heat Bal. % error |
|---|---|---|---|---|---|
| —o— | 1 | 148.4 (1.094 e5) | 1,412 (204.9) | 36.38 (98.0) | 8.57 |
| — ◇ — | 2 | 204.8 (1.511 e5) | 1,353 (196.3) | 34.97 (94.9) | 2.82 |
| · · △ · · | 3 | 309.4 (2.282 e5) | 1,748 (253.5) | 45.47 (113.9) | 7.34 |
| — □ — | 4 | 439.1 (3.238 e5) | 1,772 (257.0) | 46.05 (114.9) | 3.04 |

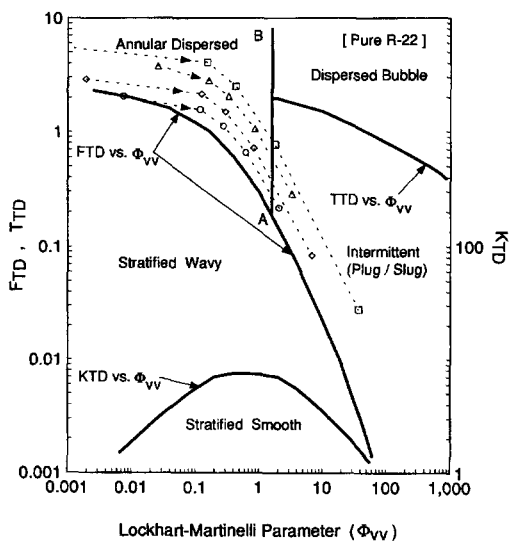


Fig. 4. Variation of the flow regimes for condensation of R-22 at different mass flux rates (Taitel and Dukler [3]).

it can be noticed that most of the points at which the local $h$ values are calculated [i.e. locations 2–4 in Fig. 3(a)] are in annular flow regime, except for the curve with the lowest mass flux rate which are close to the transition line. Hence this suggests that the assumption of annular flow for the model development is a valid one.

Figure 5(a)–(d) shows the graphs for four particular test runs in which the local heat transfer coefficient, obtained both experimentally and analytically, is plotted against the quality. The four graphs are in the increasing order of the mass flux rate $G$, although the condensing temperatures (or the saturation pressures) are not same. It is observed in this study (see Chitti [29] for a detailed discussion) that the condensing temperature did not play an important role in the local $h$ values. Also the local $h$ values as calculated by four correlations reported in the literature are plotted in each case.

As can be seen from the graphs, the predicted values are in good agreement with the experimental results except for the lowest mass flux rate [Fig. 5(a)]. However, it can be noticed from Fig. 5(a) that the prediction of the analytical model is in agreement with the other correlations, all of which are under predicting the local $h$ by approximately same amount. It is also observed in this study that the experimental uncertainty for low mass flux rates has been higher as it involved more error in evaluating the mass flow rate during calibration. In other words, the actual values might lie somewhere in between the predicted and experimental values. This disagreement can also be understood from the flow regime point of view. From Fig. 4, it can be noticed that the curve for the lowest

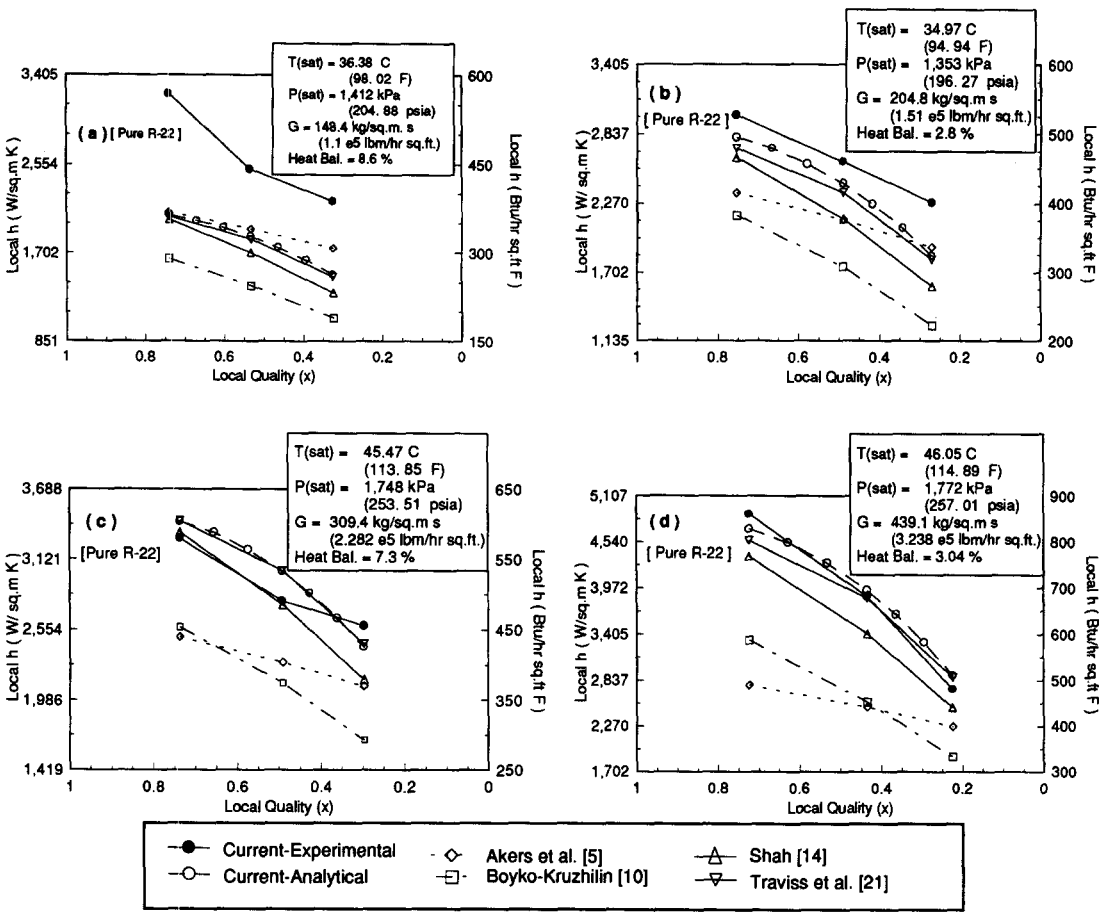


Fig. 5. Variation of local heat transfer coefficient with quality for R-22.

mass flux rate in Fig. 5(a) follows closely the transition line $F_{TD}$ vs $\phi_{vv}$. This suggests that the flow regime could actually be stratified wavy rather than dispersed annular. Hence if the condensing fluid were to be in stratified wavy flow regime, there would be a non-uniformity in the heat transfer occurring around the circumference of the tube. But the experimental values were calculated assuming uniform heat transfer rate (one-dimensional conduction model) which might be causing the large errors seen in Fig. 5(a). Also, the close agreement of the experimental and predicted local $h$ values for higher mass flux rates [Fig. 5(b)–5(d)] supports the above argument. This is because, for Fig. 5(b)–5(d), the flow regime curves in Fig. 4 indicate a fully dispersed annular flow except at the low qualities. This in turn implies uniform heat transfer rate around the circumference of the tube and hence less errors in the assumption of one-dimensional conduction model for evaluating local $h$ values.

Further, the current model is in close agreement with Shah [14] and Traviss *et al.* [21] correlations in comparison with those of Akers *et al.* [5] and Boyko-Kruzhilin [10]. Both Akers *et al.* [5] and Boyko-Kruzhilin [10] correlations have been observed to underpredict the local $h$ values by several researchers as reported by Shah [14]. One reason could be because both the researchers tried to improve a chosen single-phase heat transfer correlation by suitably adding modifying factor(s). The modifying factor involved was the equivalent mass velocity ($G_e$). But this modifying factor alone may not be able to incorporate all the parameters influencing the local heat transfer coefficient. In other words, they do not have a strong physical basis of the complex two-phase condensation phenomena.

Figure 6(a)–(d) shows the graphs for the predicted values of the actual ($\delta$) and non-dimensional ($\delta^+$) film thickness, on the primary and secondary axes, respectively, corresponding to the testing conditions of Fig. 5(a)–5(d). As expected the $\delta$ values are physically realistic and its trend with the local quality is as expected. In other words, the film thickness $\delta$ increases in the flow direction because more of the fluid is condensing and the quality is decreasing in that direction. It may also be noted from Fig. 6(a)–(d) that the non-dimensional film thickness $\delta^+$ is varying linearly with the local quality $x$. But the actual film thickness $\delta$ is not varying linearly. Its gradient in the flow direction is higher for qualities lower than 50% than for qualities above 50%. This explains the reason for the increased thermal resistance in the liquid film at lower qualities causing greater decrease in the heat transfer.

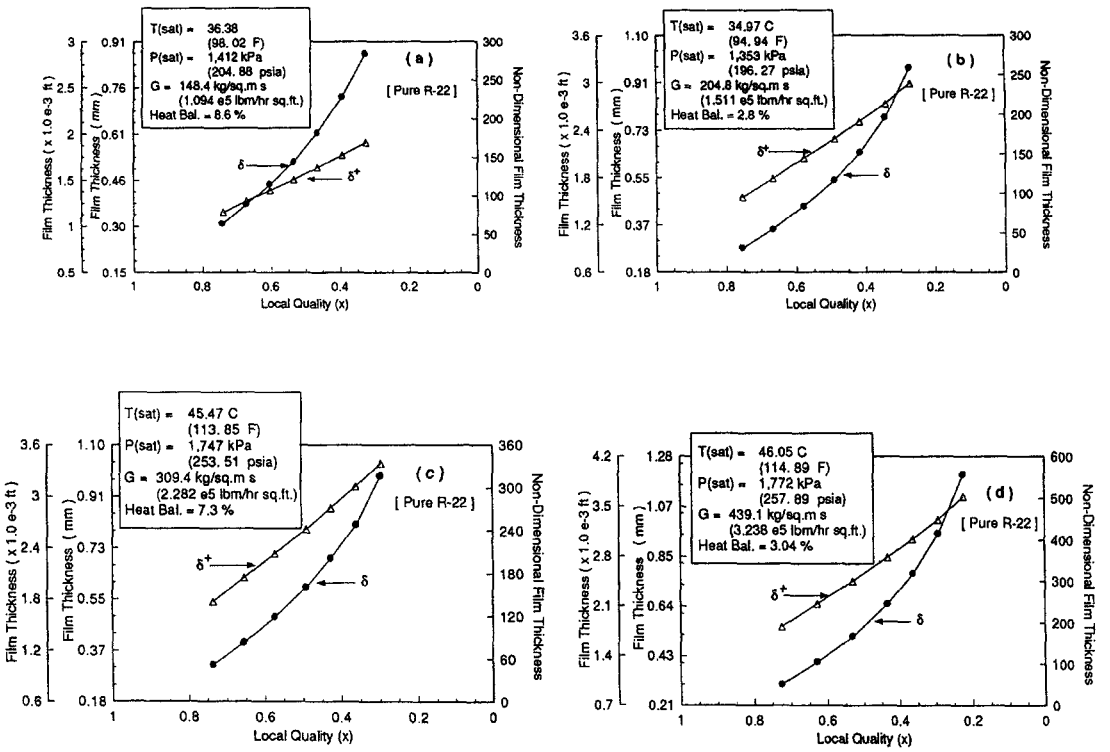


Fig. 6. Variation of dimensional ($\delta$) and non-dimensional film thickness ($\delta^+$) with quality for R-22.

All the correlation models plotted in Fig. 5(a)–(d) seem to support this trend for local $h$. The experimental results also, except that of lowest mass flux rate [Fig. 5(a)], indicate that the local $h$ value decreases rapidly for qualities lower than 50%. And, the trend seems to be same for all the four mass flux rates plotted.

The exponential increase in the film thickness can be understood from the flow regime map of Fig. 4 wherein it can be noticed that all the curves tend to remain horizontal until a certain value of the Lockhart–Martinelli parameter ($\phi_{vv}$) and thereafter drop rapidly. These values are approximately between 0.4 and 0.5 which correspond to local qualities of about 0.5. This sudden drop in the value of $F_{TD}$ for qualities less than 0.5 also indicates that the gravitational force on the liquid film is increasing exponentially relative to the vapor velocity. This in turn confirms that the liquid film thickness has to increase non-linearly and rapidly for qualities less than 0.5.

The above trend in the liquid film thickness can also be inferred from the definition of $y^+$ in equation (7b). It can be noticed that $\delta^+$ is a measure of the wall shear stress which decreases exponentially in the flow direction for internal turbulent flow. This implies that, for a linear increase in $\delta^+$, the actual film thickness $\delta$ should increase non-linearly. This non-linear increase in $\delta$ is required due to the fact that the $\tau_0$ varies to the one-half power in the expression for $\delta^+$.

Figure 7(a)–(d) shows the graphs for comparison of analytically predicted local heat transfer coefficient values by different correlations with that of the experimental results obtained in this study. Figure 8 shows the comparison of the present model with that of the experimental data. For each of the correlation method, the deviation in the local $h$ value is calculated at every data point as follows:

$$e_{per} = \frac{|h_{exp} - h_{calc}|}{h_{exp}} \tag{28}$$

and the mean deviation $e_{av}$ is then calculated by

$$e_{av} = \frac{1}{n}\left(\sum_{1}^{n} \frac{|h_{exp} - h_{calc}|}{h_{exp}}\right) \times 100 \tag{29}$$

where $n$ is the number of data points at which local $h$ is calculated. In Fig. 7(a), it can be seen that Akers *et al.* [5] correlation gives reasonable values for low mass flux rates only and deviates very much for higher mass flux rates. Mostly, the values are underpredicted even for low mass flux rates. Also the mean deviation is calculated as 21.5%. But Boyko-Kruzhilin's correlation [10] plotted in Fig. 7(b) shows that their correlation under predicts throughout the range of the experimental data by about 25%. This can also be verified from the mean deviation which is calculated as 26.2%. These observations are supported by the arguments proposed by Shah [14]. Figure 7(c) and (d)

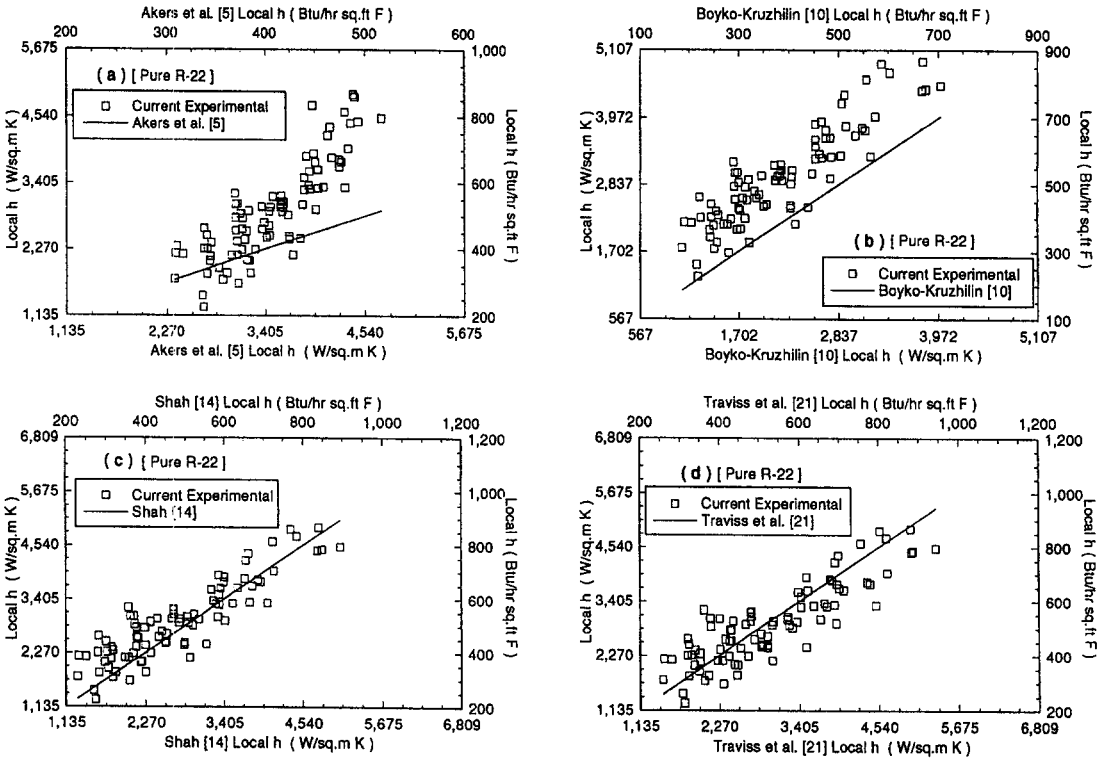


Fig. 7. Comparison of current experimental data with different correlations for R-22.

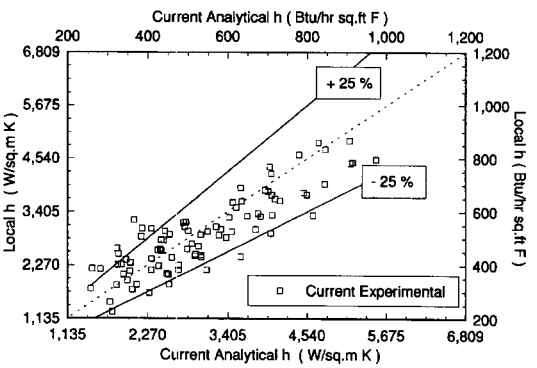


Fig. 8. Comparison of current analytical model with current experimental data for R-22.

shows the plots for Shah [14] and Travis *et al.* [21] correlations which are having an even distribution of the experimental data points about the predicted values. The mean deviations are calculated as 13.3 and 14.6%, respectively, which are far better than the deviations of the other two correlations. These two correlations are based on a very detailed analysis involving several key parameters such as the shear stress and pressure drop and void fraction. Hence their agreement with the experimental data is as expected.

Figure 8 shows the comparison of the analytical model developed in the current study with that of experimental results. It indicates that most of the experimental values are within a range of $\pm 25\%$ of the predicted values with a mean deviation of 15.3%. This is very close to the mean deviation values of those of Shah [14] and Traviss *et al.* [21] correlations, although it is slightly greater than theirs. But it is significantly less than those of Akers *et al.* [5] and Boyko-Kruzhlin [10] correlations. This shows that the present analysis is simpler to use than those of Shah [14] and Traviss *et al.* [21] correlations and that its predictions match closely with theirs.

In summary, the comparison of the predictions of the current analytical model with the experimental results and other correlations indicate that the model can be used to predict the local heat transfer coefficients within $\pm 25\%$. This gives the confidence that the model has good predicting capability. This also suggests that, since the model is based on a semi-theoretical approach, the local $h$ values can be predicted reasonably well for a wide variety of conditions.

## CONCLUSIONS

(1) A simple calculation procedure for predicting the local heat transfer coefficients during two-phase forced convective condensation is proposed for annular flow configuration.

(2) It can be said that the Prandtl mixing length theory in combination with Van-Dreist's hypothesis [22] for the continuous law of the wall model for

evaluating the eddy viscosity for momentum simplifies the problem to a great extent.

(3) The current procedure although involves an iteration procedure to calculate the film thickness, eliminates the calculations of void fraction, pressure drop and shear stress distribution.

(4) The results indicate that the predicted values of local heat transfer coefficients for R-22 agree well with the experimental data to within $\pm 25\%$, with a mean deviation of 15.3%.

(5) The mean deviation value obtained is much lower than the correlations of Akers *et al.* [5] (21.5%) and Boyko-Kruzhilin [10] (26.2%) while it is slightly more than those of Shah [14] (13.3%) and Traviss *et al.* [21] (14.6%) correlations.

*Acknowledgements*—This research, supported by the Texas Higher Education Coordinating Board under the Texas Advanced Technology Research Program (TARTP) (Project No. 32131-70640) and by the ASHRAE in the form of Graduate Student-in-Aid Fellowship is greatly acknowledged. Inputs of Dr D. L. O'Neal of Texas A&M University and Dr L. Swanson of HTRI are greatly appreciated.

## REFERENCES

1. M. Soliman and N. Z. Azer, Flow patterns during condensation inside a horizontal tube, *ASHRAE Trans.* **77**(1), 210–224 (1971).
2. W. F. Stoecker and D. DeGrush, Measurements of heat-transfer coefficients of nonazeotropic refrigerant mixtures condensing inside horizontal tubes, Oak Ridge National Laboratory/Sub/81-7762/6 and 01 (1987).
3. Y. Taitel and A. E. Dukler, A model for predicting flow regime transitions in horizontal and near horizontal gas–liquid flow, *A.I.Ch.E. Jl* **22,** 47–55 (1976).
4. L. V. Abis, Forced convective condensation inside horizontal tubes, Ph.D. Dissertation, Kansas State University, Manhattan, KS (1969).
5. W. W. Akers, H. A. Deans and O. K. Crosser, Condensation heat transfer within horizontal tubes, *Chem. Engng Prog. Symp. Ser.* **55**(29), 171–176 (1959).
6. W. W. Akers and H. F. Rosson, Condensation inside a horizontal tube, *Chem. Engng Prog. Symp. Ser.* **56**(30), 145 (1960).
7. M. Altman, F. W. Staub and R. H. Norris, Local heat transfer and pressure drop for Refrigerant-22 condensing in horizontal tubes, *Proceedings of ASME–AIChE Heat Transfer Conference*, Storrs, Connecticut, 151–159 (1960).
8. S. Bae, J. S. Maulbetsch and W. M. Rohsenow, Refrigerant forced convection condensation inside horizontal tubes, Department of Mechanical Engineering, Heat Transfer Lab., Report No. 79760-59, MIT, Cambridge, MA (1968).
9. S. Bae, J. S. Maulbetsch and W. M. Rohsenow, Refrigerant forced convection condensation inside horizontal tubes, Department of Mechanical Engineering, Heat Transfer Lab., Report No. 79760-64, MIT, Cambridge, MA (1969).
10. L. D. Boyko and G. N. Kruzhilin, Heat transfer and hydraulic resistance during condensation of steam in a horizontal tube and in a bundle of tubes, *Int. J. Heat Mass Transfer* **10,** 361–373 (1967).
11. J. Chaddock, Film condensation of vapor in horizontal tubes, *Refrigerating Engng* **65**(4), 37 41–44 (1957).
12. J. Chato, Laminar condensation inside horizontal and inclined tubes, *ASHRAE Jl* 52–60 (February 1962).
13. H. F. Rosson and J. A. Myers, Point values of condensing film coefficients inside a horizontal pipe. *Chem. Engng Prog. Symp. Ser.* **59,** 190–199 (1963).
14. M. M. Shah, Heat transfer during film condensation in tubes and annuli: a review of the literature, *ASHRAE Trans.* **87**(1), 1086–1105 (1981).
15. M. Soliman, J. R. Schuster and P. J. Berenson, A general heat transfer correlation for annular flow condensation, *ASME J. Heat Transfer* **10,** 267–276 (1968).
16. H. R. Kunz and S. Yerazunis, An analysis of film condensation, film evaporation, and single-phase heat transfer for liquid Prandtl numbers from $10^{-3}$ to $10^{4}$, *ASME J. Heat Transfer* **91,** 413–420 (1969).
17. W. Z. Nusselt, Die oberflachen kondensation des wasser damper, *Z. Ver. dt. Ing.* **60,** 541–569 (1916).
18. M. Jakob, Heat transfer in evaporation and condensation, *Mech. Engng* **58,** 729 (1936).
19. E. F. Carpenter and A. P. Colburn, Proceedings of General Discussion on Heat Transfer, *Inst. Mech. Engrs Am. Soc. Mech. Engrs* 20–26 (July 1951).
20. N. Z. Azer, L. V. Abis and H. M. Soliman, Local heat transfer coefficients during annular flow condensation, *ASHRAE Trans.* **84,** 135–143 (1978).
21. D. P. Traviss, W. M. Rohsenow and A. B. Baron, Forced-convection condensation inside tubes: a heat transfer equation for condenser design, *ASHRAE Trans.* **79**(1), 157–165 (1973).
22. W. M. Kays and M. E. Crawford, *Convective Heat and Mass Transfer* (2nd Edn). McGraw-Hill, New York (1980).
23. V. P. Carey, *Liquid–Vapor Phase Change Phenomena.* Hemisphere, New York (1992).
24. J. A. Tichy, N. A. Macken and W. M. B. Duval, An analytical model for condensing and evaporating two-component two-phase annular flow, *Proceedings of the Seventh International Heat Transfer Conference*, Vol. 5, pp. 161–166 (1982).
25. R. C. Downing, Refrigerant equations, *ASHRAE Trans.* **80**(2), 158–169 (1974).
26. G. T. Kartsounes and R. A. Erth, Computer calculation of the thermodynamic properties of refrigerants, 12, 22 and R-502, *ASHRAE Trans.* **77,** 88–103 (1971).
27. J. H. Kim, T. W. Simon and R. Viskanta, *Journal of Heat Transfer* policy on reporting uncertainties in experimental measurements and results (Editorial), *ASME J. Heat Transfer* **115**(1), 5–6 (1993).
28. S. J. Kline and F. A. McClintock, Describing uncertainties in single-sample experiments, *Mech. Engng* **75,** 3–8 (1953).
29. M. S. Chitti, Condensation of a new alternative refrigerant flowing inside horizontal smooth tubes, Ph.D. Dissertation, Texas A&M University, College Station, TX (August 1994).

## APPENDIX A

*Van-Dreist's hypothesis* [22]

The mixing length '$l$' is given by

$$l = \kappa y\left[1 - \frac{1}{e^{(y^+/A^+)}}\right] \tag{A1}$$

where

$\kappa = 0.4$ (Von-Karman's constant for pipe flow)

$A^+ = 26.0$ (constant for pipe flow).

By the definition of $\varepsilon_m$, we have

$$\varepsilon_m = l^2\left|\frac{du}{dy}\right|. \tag{A2}$$

Substituting for '$l$' from equation (A1) into the above equation (A2), we get

$$\varepsilon_m = \kappa^2 y^2 \left[1 - \frac{1}{e^{(y^+/A^+)}}\right]^2 \left|\frac{du}{dy}\right|. \quad \text{(A3)}$$

Equation (A3) in a non-dimensionalized form can be written as

$$\frac{\varepsilon_m}{\nu_l} = \kappa^2 (y^+)^2 \left[1 - \frac{1}{e^{(y^+/A^+)}}\right]^2 \left|\frac{du^+}{dy^+}\right|. \quad \text{(A4)}$$

In this equation the term $|du^+/dy^+|$ can be obtained from the Von-Karman's [24] universal velocity distribution given by

$$u^+ = y^+, \quad 0 < y^+ < 5 \quad \text{(A5)}$$

$$u^+ = -3.05 + 5.0 \ln (y^+) \quad 5 \leqslant y^+ \leqslant 30 \quad \text{(A6)}$$

$$u^+ = 5.5 + 2.5 \ln (y^+) \quad y^+ \geqslant 30. \quad \text{(A7)}$$

Hence $\varepsilon_m/\nu_l$ can be calculated for any $y^+$.

## APPENDIX B

*Heat flux distribution* $q/q_0$

The distribution $q/q_0$ can be obtained by the heat flux continuity in the radial direction. Neglecting axial diffusion, from the steady-state energy balance at any radial location $r$ and the tube wall $r_0$ we get

$$q(2\pi rL) = q_0(2\pi r_0 L). \quad \text{(B1)}$$

But, since $r = r_0 - y$, equation (B1) can be written as

$$\frac{q}{q_0} = \frac{r_0}{r} = \frac{r_0}{r_0 - y} = \frac{1}{\left(1 - \frac{y}{r_0}\right)} = \frac{1}{\left(1 - \frac{y^+}{r_0^+}\right)}. \quad \text{(B2)}$$

## APPENDIX C

*Uncertainty analysis*

The basic methodology followed was that of the propagation equation of Kline and McClintock [17] in accordance with the guidelines of Kim *et al.* [16]. If the result, $R$, was a function of the independent variables $(x_1, x_2, \ldots, x_n)$, the uncertainty $(\cup)$ in $R$ was expressed by the propagation equation as follows:

$$\cup_R = \{(B_R)^2 + (P_R)^2\}^{1/2} \quad \text{(C1)}$$

where $B_R$ and $P_R$ were the bias and precision limits of $R$, respectively. They were calculated by the same propagation equation as follows:

$$B_R = \left\{\left(\frac{\partial R}{\partial x_1} Bx_1\right)^2 + \left(\frac{\partial R}{\partial x_2} Bx_2\right)^2 + \ldots + \left(\frac{\partial R}{\partial x_n} Bx_n\right)^2\right\}^{1/2} \quad \text{(C2)}$$

$$P_R = \left\{\left(\frac{\partial R}{\partial x_1} Px_1\right)^2 + \left(\frac{\partial R}{\partial x_2} Px_2\right)^2 + \ldots + \left(\frac{\partial R}{\partial x_n} Px_n\right)^2\right\}^{1/2} \quad \text{(C3)}$$

where

$B_R$ = uncertainty in calculating $R$ due to bias error (fixed error)

$Bx_i$ = uncertainty in variable $x_i$ due to bias error (fixed error)

$P_R$ = uncertainty in calculating $R$ due to precision error (random error)

$Px_i$ = uncertainty in variable $x_i$ due to precision error (random error).

The expression used for the uncertainty in the heat transfer coefficient $h_i$ was

$$h_i = \frac{1}{\frac{1}{U_i} - \frac{A_i \ln (r_0/r_i)}{2\pi KL} - \frac{A_i}{A_0}\frac{1}{h_0}}. \quad \text{(C4)}$$